

Hardware and Software Improvements to a Low-Cost Horizontal Parallax Holographic Video Monitor

ANDREW HENRIE¹, JESSE R. CODLING¹, SCOTT GNEITING¹, JUSTIN B. CHRISTENSEN¹, PARKER AWERKAMP¹, MARK J. BURDETTE¹, AND DANIEL E. SMALLEY¹

¹Electrical and Computer Engineering Department, 459 Clyde Building, Brigham Young University, Provo, UT, 84602

Published November 22, 2017. Corrected 10 September, 2018

Displays capable of true holographic video have been prohibitively expensive and difficult to build. With this paper, we present a suite of modularized hardware components and software tools needed to build a Holovideo Monitor with basic "hacker-space" equipment, highlighting improvements that have enabled the total materials cost to fall to \$820, well below that of other holographic displays. It is our hope that the current level of simplicity, development, design flexibility, and documentation will enable the lay engineer, programmer, and scientist to relatively easily replicate, modify and build upon our designs, bringing true holographic video to the masses. © 2024 Optical Society of America

OCIS codes: 090.1760 Computer Holography, 090.2870 Holographic Display, 090.1970 Diffractive Optics

<https://doi.org/10.1364/AO.57.00A122>

1. INTRODUCTION

Since the introduction of leaky mode modulators for holographic video applications, a number of publications have chronicled advancements on the modulator-chip level [1–3]. One of the main applications of this device, a low-cost holographic video monitor (or "Holovideo Monitor"), has been in concurrent development. This paper seeks to achieve two objectives: (1) to provide a complete summary of the design, construction, and basic operation of such a monitor, and (2) to report on cost, stability, and performance improvements in the modulators and system, including a summary of the design and implementation of low-cost leaky mode modulators. To facilitate development and collaboration of this project, links to our design files, assembly instructions, and software repositories can be found at <http://holography.byu.edu/>. It is hoped that these resources and improvements will help enable less-equipped experimenters and researchers to more easily explore the design and implementation space of low-cost holographic video.

Our earlier prototype holographic video monitors [4–8] were sufficient in functionality to demonstrate the utility of the waveguide modulator approach, but suffered from several drawbacks, including lack of robustness and high cost. As development continued, a set of specifications [7] was established as a goal for a consumer-grade holographic display, including cost, resolution, and refresh rate. At the time, the goal to reduce the bill of materials below \$1000 was still not plausible due to several factors, the resolutions of which will be discussed here.

One such drawback was the need for expensive prisms in order to couple light into our modulators. With our improvements,

we have replaced the coupling prisms in favor of on-device input coupling gratings, producing dramatic savings in modulator cost. As we continue to develop more efficient devices, we also obviate the need for expensive power amplifiers.

Other challenges in previous designs included resolution constraints and unstable optomechanical components. In particular, the immediately previous iteration of this platform, described in [8, 9], was overly large and very difficult to align and keep aligned due to an unsteady sheet-metal chassis. This lack of robustness in the optomechanical path served as an additional constraint to any outside work on the monitor, as considerable patience and expertise were needed to use, let alone maintain, the Monitor. In our latest design, we've reduced the form factor by replacing the folded sheet-metal body and expensive optical mounts with cost-effective 3D-printed parts. These not only reduce the form factor, but also stabilize the optical alignment and establish a system of easily-replaceable optical and electrical modules.

The outline of this paper is as follows: in Section 2, we summarize scanned aperture holography and the overall architecture of the Holovideo Monitor; in Section 3, we describe design decisions that determined our implementation; in Section 4, we explain the hardware components enabling the new design; in Section 5, we discuss the software used to test and drive output imagery; in Section 6, we discuss results. Finally, in Section 7, we share our conclusion and discuss future work.

2. RECAPITULATION OF CONCEPT

Scanned aperture holographic video, pioneered at the Massachusetts Institute of Technology (MIT), is functionally an acousto-optic modulator (AOM) imaged through an optical system composed of a telescope with one or more scanners at the Fourier plane. Typical AOMs are not suitable for direct-viewing due to their low diffraction angles (with a notable exception [2, 3]) and small apertures. The first of these deficiencies is overcome by imaging through a telescope which demagnifies the aperture by a factor proportional to the ratio of the focal lengths of the telescope's optical elements. The result of demagnification in extent is a magnification in angle. The small aperture, a problem exacerbated by demagnification, is overcome by placing a scanning optic (e.g. a galvanometer or polygon mirror) at the telescope Fourier plane, which scans the image of the AOM and *descans* the surface acoustic wave pattern which appears in the device aperture, making the pattern appear stationary.

This geometry has undergone a number of variations beginning with the MIT Mark I [4], which utilized a three channel Bragg cell and a large polygon scanner to achieve color video images. The Mark II [5] replaced the polygon scanner with a bank of galvanometric scanners and increased the number of channels in the Bragg cell to 18 (the Bragg cell was also duplicated to take advantage of forward and backward scanning). The Mark III [6] attempted to use a two axis waveguide scanner to eliminate the need for horizontal scanning. The Mark IV [7, 8] utilized a single multicolor leaky mode waveguide modulator fed by a prism coupler.

In our current instantiation (shown in Figure 1) we have introduced grating input couplers to eliminate the need for a coupling prism. The current geometry also has the flexibility of supporting either one multicolor modulator or three single color modulators. Each modulator is part of a cartridge system, leading to modularity and further flexibility. Taken together, these improvements greatly reduce the volume of the supporting optics and electronics. The architecture is also much more robust and less expensive than previous iterations. As this development has occurred at Brigham Young University (BYU), we have dubbed this most recent architecture the BYU/MIT Mark V, as it represents the continued work from earlier platforms developed at MIT.

Monitors using this holographic video method effectively constitute a display with a short vertical resolution and an extremely dense horizontal resolution spread over an angular range. By controlling the timing and frequency content of the signal sent to our modulators, we can control the output intensity (and thus color) and projection angle of light coming out of the two-dimensionally scanned output (compared with normal screen pixels which project a single color in all directions). Frequency chirps can be used to recreate arbitrary point holograms. Multiple signals can be linearly added together to create compound light structures, such as stereograms or holograms. While no vertical parallax is present (due to the one-dimensional nature of AOM fringe patterns), stereopsis from horizontal parallax and accommodation cues can still be generated, recreating true three-dimensional (3D) imagery.

3. DESIGN DECISIONS

The current Monitor design is built to be flexible. Many design decisions are simply trade-offs in capabilities, ease of use, and cost. The type of modulator employed in a system heavily influences other design decisions. For example, a previous modulator

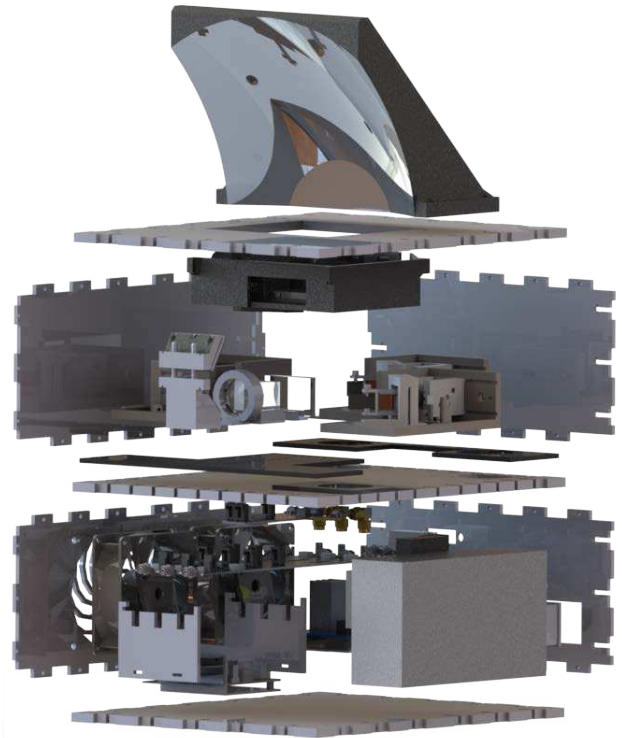


Fig. 1. An exploded view of the Mark V Holographic Video Monitor. The upper internal level contains the optics, and the lower internal level contains the electronics.

design coupled multiple laser wavelengths into a single modulator, which were then differentiated by separate bands of interaction frequency. This Frequency-Division Color-Multiplexing (FDCM) approach is very efficient in terms of space and signal bandwidth, but was discarded in favor of a simpler arrangement when simultaneous alignment became too tedious. In modulators specializing in one wavelength, only a single modulator channel is used for each color, again, for simplicity in optical design. Another modulator design factor, the number of internal parallel channels, also effects other bandwidth requirements and potential vertical resolution. Both FDCM and multichannel modulator design may be re-visited as development continues.

A. Optical Path

New lower-cost modulators, achieved by grating input coupling, provided an opportunity to tackle many of the shortcomings of previous iterations. The majority of the volume of older designs was dominated by large optical assemblies for precise control of alignment. By developing a modular, space-conserving cartridge design for our devices, we were able to reduce the optical path and utilize separate modulators optimized for different wavelengths.

The optical path (shown in Figure 2) begins with our newly designed modulator cartridges. Each cartridge sweeps a single beam color into a tricolor (RGB) dichroic prism cube (with a rectangular prism used to center the green channel with the cube). All three color beams are redirected forward as a combined beam through the transform lens. The resulting beam is directed upwards towards a polygon mirror for horizontal scanning. The polygon mirror's facets rest at the focal point of the transform lens, forming the Fourier plane of a telescope

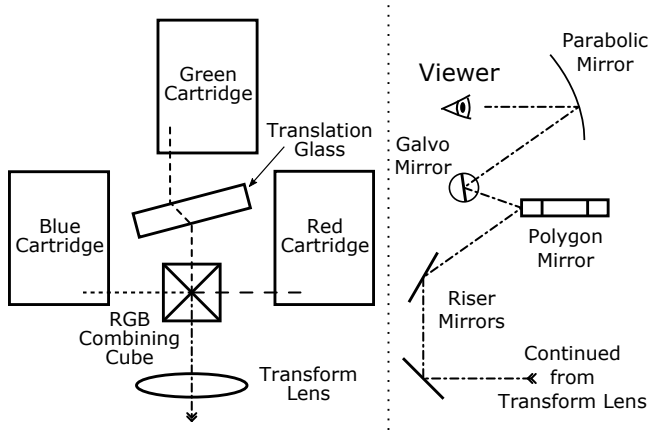


Fig. 2. A diagram of the Mark V optical path. On the left is a top-down view showing the optics path through the transform lens. The right is a side profile of the remainder of the optical path.

system between the transform lens and parabolic reflector. From the polygon mirror, the light is reflected to a galvanometer for vertical scanning and finally directed forward from a parabolic mirror. Without a vertical diffuser, images are restricted to a single view plane (directly forward, parallel to the monitor’s base).

One notable change in this optics setup is the divergence from FDCM modulators used in Mark IV iterations involving leaky-mode devices. At the time, with the expense of coupling prisms for older modulators, it was more efficient to couple the three necessary colors into a single modulator. While advantageous at the time, our new input coupling gratings couple different light wavelengths at different input angles relative to a grating of a compatible pitch. If in the future FDCM modulators are desired, a series of gratings could be used to couple a series of converging beams of different wavelengths into a single waveguide.

The new design is effective and simple, relative to previous attempts. It’s advantages include ease of alignment, stability, and permanence once assembled; the system is sturdy enough that it can maintain alignment even if handled and moved. Additionally, it is highly modular, with inexpensive, replaceable components should damage or failure occur, contributing to a more developer and user friendly system.

B. Bandwidth Trade-Offs

The analog data pipe to the monitor is limited by several factors which influence design decisions. Consumer graphics cards, which drive the Monitor, have bounds to their pixel clock and active pixel ranges, determined by hardware capability and driver limitations. The scanning system also has mechanical constraints (such as maximum polygon motor speed). In the following equations we lay out the bandwidth relations governing the display parameters, followed by a listing of these constraints.

$$f_{GPU} = H_{Total} * V_{Total} * f_{Framerate} \tag{3.1}$$

$$H_{Total} = \frac{f_{GPU}}{f_{HSYNC}} \tag{3.2}$$

$$H_{Active} = H_{Total} - H_{BlankMin} \tag{3.3}$$

$$f_{HSYNC} = f_{Poly} * N_{CRHL} \tag{3.4}$$

$$V_{Total} = N_{HoloLines} * N_{CRHL} \tag{3.5}$$

$$V_{Active} = V_{Total} - V_{BlankMin} \tag{3.6}$$

$$f_{Poly} = f_{Framerate} * N_{HoloLines} \tag{3.7}$$

$$f_{Poly} = \omega_{Poly} * N_{Facets} \tag{3.8}$$

H_{Active} , $H_{BlankMin}$, H_{Total} , V_{Active} , $V_{BlankMin}$, and V_{Total} are pixel counts in the active, blanking, and total screen regions in the horizontal and vertical dimensions respectively. f_{GPU} , also called the Graphics Processing Unit (GPU) pixel sampling rate or clock, is the frequency at which new pixels’ information is transmitted (not the same as the rate of pixel calculation). $f_{Framerate}$ is the refresh rate of the image. f_{HSYNC} and f_{Poly} are the scan frequencies of computer rows and polygon facets (as measured using a tachometer), respectively. f_{Poly} is determined by the rotation rate of the polygon motor, ω_{Poly} , and the number of facets of the polygon, N_{Poly} . $N_{HoloLines}$ is the number of visible Holographic Monitor rows (HoloLines), or the Monitor’s vertical resolution. N_{CRHL} is the number of computer rows per HoloLine. These values are constrained as follows:

- $f_{GPU} \leq 400MHz$, the maximum sample rate of the GPUs in use.
- $H_{Active}, V_{Active} < 4096$, determined by the Extended Display Identification Data (EDID) Standard ([10]). H_{Active} must be an integer multiple of 32 (potentially from cache block sizes; determined by experimentation).
- H_{Total} must be an integer ratio of f_{GPU} / f_{HSYNC} .
- $H_{BlankMin} \geq 112$ and $V_{BlankMin} \geq 35$, determined by experimentation. This may vary between GPU products.
- $N_{CRHL} \geq 1$ and must be a divisor synthesizable in external hardware (the scanning system divides the horizontal sync signal pulse by this number).
- f_{Poly} has a practical upper limit and must be lockable.

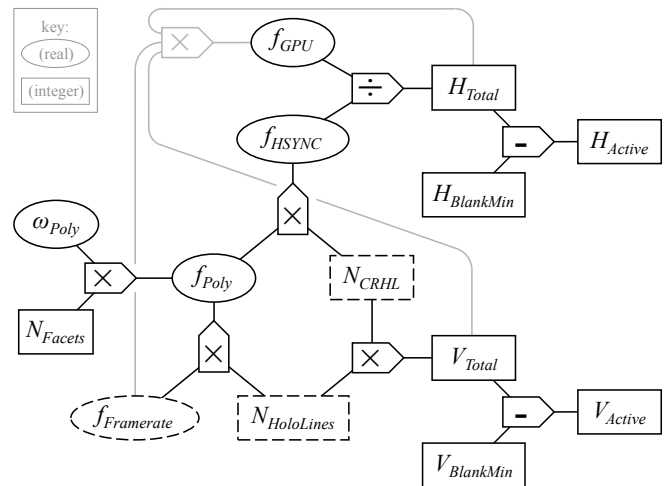


Fig. 3. The interdependence of screen variables are shown. The key in the upper-left corner specifies numerical type. Dashed lines indicate base degrees of freedom.

As these values are interdependent, we’ve included a diagram visualizing the relationships between them in Figure 3.

The relationships distill down to three base degrees of freedom: $f_{\text{FrameRate}}$, currently targeting approximately 30 FPS to match basic video standards, N_{CRHL} , and $N_{\text{HoloLines}}$. Tradeoffs could be made to sacrifice framerate for vertical resolution if desired. These base degrees of freedom are outlined with dashed lines in Figure 3.

To determine parameter values, we began with the largest possible output window and highest possible GPU sample emission frequency (constraints determined by current hardware), set degrees of freedom, evaluated proximate parameters from constraints and available performance, and back-adjusted all values as necessary to meet all constraints. This led to the current display parameter values presented in Table 1.

Table 1. Display Parameter Values

f_{GPU}	400	MHz	N_{CRHL}	64
f_{HSYNC}	100.402	kHz	$N_{\text{HoloLines}}$	52
$f_{\text{FrameRate}}$	30.169	FPS	N_{Facets}	6
f_{Poly}	1,568.8	Hz	ω_{Poly}	15,688 RPM
H_{Active}	3872	pixels	V_{Active}	3293 rows
H_{BlankMin}	112	pixels	V_{BlankMin}	35 rows
H_{Total}	3984	pixels	V_{Total}	3328 rows

4. HARDWARE COMPONENTS

A. Input Coupling Gratings

Reviewing our modulator design (see Figure 4 and [1, 11–15] for more detail), we embed light-transmitting waveguides in small samples of X-cut lithium niobate (LiNbO_3 , approximately 10mm wide, 14mm long, and either 1.0mm or 3.0mm thick, generally with 6 channels on each device) before depositing aluminum transducers along the Y-axis via traditional photolithography processes. These transducers are placed at one end of the waveguides along the same axis. The mechanism for coupling light into the waveguide exists on the opposite end of the waveguide. The transducers are wire-bonded to a connector breakout board, to which computer-controlled RF driving electronics are connected.

These RF signal sources, connected to the transducers, cause the underlying LiNbO_3 to expand and contract due to the piezoelectric effect, generating surface-acoustic waves (SAWs) that propagate contra-collinear to the light traveling in the waveguide. The frequencies of these SAWs are such that light in the waveguide leaks out and diffracts at controlled angles. We label the region where SAWs overlap light trapped in the waveguide as the "interaction region". The range of frequencies that interact with red, green, and blue light exist between approximately 340 to 550 MHz, depending upon several waveguide and transducer fabrication parameters.

In order to couple light into the waveguide, sufficient momentum must be added to the incoming light as to allow it to propagate down a particular waveguide mode. In previous modulator iterations, a rutile (titanium dioxide) prism was used to couple light into the waveguide. This prism, however, cost \$478 per 62 mm^3 sample, required careful installation and alignment, and was easily damaged.

We replaced the expensive rutile prism by etching input-coupling gratings (one per waveguide channel) into the lithium niobate at the beginning of each waveguide. As the light enters in the side of the device, it continues on to hit a grating from underneath, then bends directly into the corresponding waveguide. Manufacturing these gratings is cost-minimal, as they constitute only a small modification to the lithography process used to create the waveguides and transducers.

The period of the grating is optimized for each wavelength of light to ensure that an optimal entry angle for the corresponding color is possible. These gratings have a depth of 350nm, a fill factor (duty cycle) of 50%, and are currently 15% efficient (the rutile prisms were only 2% efficient). We have experimentally determined the range of optimal grating pitches to be $4.19\text{--}6.00\mu\text{m}$ for red (650nm) light, $3.83\text{--}5.43\mu\text{m}$ for green (532nm) light, and $4.19\text{--}5.74\mu\text{m}$ for blue (450nm) light, when interacting with the gratings from the bottom. The range of input angles for those periods is between 27 and 45 degrees.

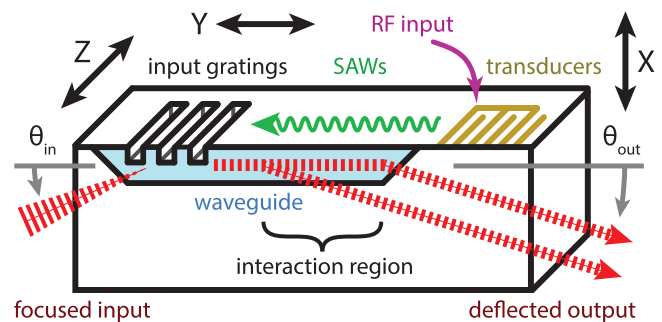


Fig. 4. Cut-away view of our modulator design, with input-coupling gratings (left), waveguide (left to center), and transducers (right) fabricated on a LiNbO_3 substrate.

Using the input coupling gratings, the expensive rutile prism and its cumbersome mounting hardware is no longer needed. As the modulator development process applies to an entire LiNbO_3 wafer, the materials cost of each modulator falls to only a few dollars (we estimate that it could be as little as \$5 to \$10 per chip), given the large number that can fit onto a single wafer. The packaged size of each modulator is constrained only to that which is necessary to wirebond RF connector breakout boards and to align incoming laser light.

B. Modulator Cartridge

The most critical optical alignment in the Monitor is the laser-to-modulator alignment. Light from a laser module must be focused down onto the input coupling grating, which has an area of approximately 0.25 to 1 mm^2 (a factor still being optimized). If this alignment is not maintained, no modulated light will be produced. Previously, with rutile prism coupling, large metallic standoffs and optics breadboards were used to hold the lasers and modulators in place relative to each other. The modulator alignment process could sometimes last several hours. This system was also extremely susceptible to falling out of alignment due to vibration or thermal expansion/contraction, and required realignment every couple of weeks. Transportation was almost impossible without losing alignment.

The frustration of having to repeatedly realign the modulators led us to design a modular 3D-printed cartridge which could be readily replaced if anything damaged the modulator

or affected the internal alignment. Once aligned, the cartridge elements are fixed permanently, making the alignment resistant to vibrations. Its small form factor also makes the alignment less susceptible to thermal expansion. A rendering of one of these cartridges is shown in Figure 5. We use a FormLabs Form 2 3D SLA printer to print our cartridges and other mounts requiring precision greater than that which filament printers can produce.

To create full-color images, modulators optimized for different wavelengths (red, green, and blue light) are installed in separate cartridges. The design of each cartridge differs slightly based upon the desired output angle, determined by the characteristics of the color combiner cube used to combine their outputs. The configuration difference between the red and green cartridge is simply an adjustment of the final exit mirror to project light in the correct direction. Blue cartridges must be physically a mirror image of the red in order to achieve an exit angle 180° different. Red and blue cartridges' output is centered along the minor axis of the cartridge, and green cartridges' output is centered along the major axis to direct light into the combining cube.

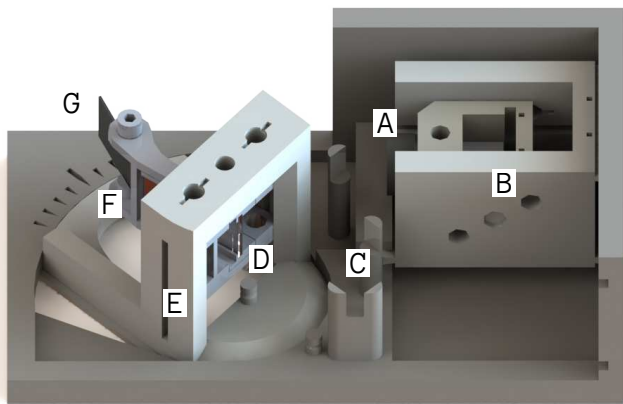


Fig. 5. A dimetric rendering of the cartridge.

These cartridges are relatively compact (measuring approximately $110\text{mm} \times 70\text{mm} \times 40\text{mm}$), and provide 3 axes of translation and one of rotation. The internal optical path begins with a diode laser (position A in Figure 5, mostly obscured). The laser is nestled within a two-axis translational mount (B), giving freedom to move the diode along the horizontal axes. Following that, a series of mirrors (C) redirect the beam to enter the modulator device (D) at long focal lengths to improve coupling efficiency (further described below). The AOM sample itself is mounted to a vertical translation mount within a rotational stage (E), providing the third axis of translation and singular axis of rotation. The translation axes account for imperfections in part printing and sample mounting, and give the freedom to select channels on a multichannel modulator. The rotational stage allows for variations in precise input angle for each device, which is dependent on exact wavelength of light and grating pitch. The AOM receives RF signals from the graphics card through a U.FL / UMCC array breakout board (F, mostly obscured), and the output is redirected as needed with a final exit mirror (G).

Each cartridge can be internally aligned separately (adjusting to maximize coupling efficiency), then installed and aligned in the optics deck of the monitor. The final exit mirror has over 300° of rotational freedom to redirect AOM output into the RGB combiner cube. Once all three cartridges are aligned

with the cube, the remainder of the optical path can be aligned using the combined beam. Old modulators or cartridges can be easily replaced by new ones if faults or better designs are found. Restoring alignment then only requires aligning the new cartridge with the combiner cube.

The use of the redirecting mirrors (C) for the input laser stems from the need for longer focal length lenses to feed the input gratings. Short focal length lenses create sufficiently large angles to inhibit coupling into valid waveguide modes. Additionally, we found by experimentation that defocusing the beam slightly (by about 5% of the total focal length of the lens) improved coupling by flooding the entire grating with moderately less intense light as opposed to a single point of highly focused light. We experimentally determined optimal focal lengths to be 60–100mm, necessitating these redirection mirrors to maintain the small form factor of the cartridge.

C. Size Reduction

Having reduced the most sensitive optical components into a modular cartridge, the large volume necessary for bulky optical alignment mounts was no longer needed, allowing the chassis size to be reduced significantly (see Figure 6). The majority of the volume in the previous design (the Mark IV [7, 8]) was occupied by these mounts.



Fig. 6. An assembled Mark V monitor is shown, with a 12-inch ruler for size comparison.

The Mark V's new design replaces those mounts with small, cheap parts designed and 3D-printed in-house (see the *Modulator Cartridge* section above), reducing both volume and cost dramatically. Using laser-cut acrylic plates as opposed to aluminum sheets reduces cost slightly, while greatly increasing workability. Individual plates can be cut and replaced as needed for modularity during development.

The reduced volume introduces another advantage to our platform: portability. As long as a sufficiently powerful computer with analog graphics capability is available to drive it, this

Holovideo Monitor need not be confined to lab environments. While previous designs were large, heavy, and cumbersome, this platform can be transported and assembled by hobbyists or consumers as well as experienced researchers.

D. Electronics Subsystems

The electronic components of the monitor are categorized into two sections: a set of radio-frequency (RF) upconversion, filtering, and amplification chains, and a digital / low-frequency analog scanning synchronization control system. The RF chain frequency-shifts and amplifies analog graphics card signals to the frequency and amplitude range needed by the acousto-optic modulators. For this, these RF chains are referred to as "Mix-Amp" (Mixer-Amplifier) chains. There can be a variable number of RF chains depending upon the number of AOM channels to be driven. The synchronization system controls the scanning optical elements to produce a stationary image based upon the graphics card's output. There is one synchronization system per Monitor.

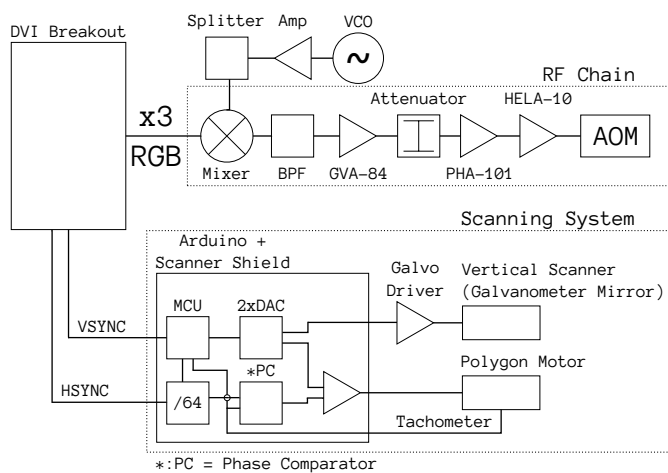


Fig. 7. Block diagram of the RF chain and synchronization system. One DVI Breakout circuit board supports up to three RF (MixAmp) chains and one scanning system.

E. Radio Frequency Upconversion Chain

The MixAmp upconversion and amplification chain uses the red, green, and/or blue analog signal channels of consumer analog graphics cards as an RF signal source. These graphics cards are hosted in high-performance commodity consumer computers. The Holovideo Monitor is seen by the host computer as a regular (4K) desktop monitor. Any graphics card that supports a VGA (Video Graphics Array), DVI-I (Digital Visual Interface-Integrated), or DVI-A (DVI-Analog) output interface is an analog graphics card and may be used. We use NVIDIA graphics cards (specifically, but not limited to, the Quadro FX 5800) because most of the NVIDIA brand's analog-capable graphics cards have a maximum digital-to-analog converter (DAC) sample rate of 400 MHz, capable of producing frequencies between 0 and 200 MHz, according to the Nyquist Theorem. This amount of bandwidth is needed in FDCM configurations where we drive red, green, and blue modulation simultaneously with a single signal and MixAmp channel (see [14, 16]).

The signal typically produced by the analog graphics card ranges between 0 to -6 dBm and has a source impedance of 75Ω. The signal voltage range is 0.0-0.7 V. Our AOMs operate between

340-550MHz, with optimal power levels between +20 and +30 dBm. The exact frequency range used for controlling each wavelength of light depends upon the modulator type, waveguide and transducer construction parameters, entry angle, optical output power profile of the modulator, and optical apertures elsewhere in the Monitor. A more precise example of aligned frequency ranges, within an FDCM modulator, is 371-404 MHz for 635nm red light, 436-474 MHz for 532nm green light, and 504-550 MHz for 445nm blue light across a 15-degree output range.

Referring to Figure 7, the DVI Breakout board breaks out the digital and analog (RF) signals from a DVI-I connector. The red, green, and blue channels are 75Ω-to-50Ω impedance-matched with a resistor network and are passed through a DC-blocking capacitor. Our RF components have an impedance of 50Ω. The DC blocking capacitor is placed after the impedance-matching resistor network so that the graphics card can pass a DC sense current to enable its analog outputs.

After the DVI Breakout segment, the RF signals pass through an RF upconverter. We use a MiniCircuits ADE-2 frequency mixer for upconversion, using the "RF" pin as the input, "IF" pin as the output, and the "LO" pin as the carrier signal input. The carrier signal typically used is 350 MHz at +7 dBm. We use a MiniCircuits ROS-535 voltage-controlled oscillator (VCO) as the Local Oscillator (LO). When multiple MixAmp chains are in use (for multiple modulator channels), the LO source is passed through an amplifier (ie, a MiniCircuits GVA-81), attenuator, and splitter (ie, a MiniCircuits SCA-3-11 or a JCPS-8-10) to provide a carrier to each MixAmp chain. The DC block used in the DVI Breakout board attenuates the carrier signal to less than 20 dB relative to our desired upconverted signal.

We use a 5-pole Butterworth LC bandpass filter after the frequency mixer to eliminate both the lower side-band product of the mixer and the upper aliases of the graphics card DAC. The filter also prevents undesired signals from decreasing the effective P1dB point of later amplifiers. The design corner frequencies are 350 and 550 MHz, providing a frequency range that can accommodate red, green, and blue modulators without design change.

To amplify the signal to an ideal target level of +30 dBm, we use a cascade of three MiniCircuits amplifiers: the GVA-84, the PHA-101, and the HELA-10. Their nominal gain and P1dB points are 24 dB, 15 dB, 10 dB, and +20 dBm, +26 dBm, and +30 dBm respectively. We use this cascade of amplifiers to achieve high gain, high power output, and little compression of the signal. An attenuator is used to prevent the PHA-101 output from exceeding the HELA-10's maximum input power of +20 dBm. As implemented, our RF system's output power reaches a maximum of +30 dBm for single tones, with harmonics reaching a maximum of 0 dBm. The output of the amplifier stage is connected via detachable cables to a modulator's breakout board, where wirebonds carry the RF signal to the modulator's transducer.

The DVI Breakout segment and other segments of the RF chain are implemented on discrete circuit boards to be developer-friendly; allowing for design flexibility and for ease of construction and testing. Previous implementations on unified, monolithic boards were difficult to test, and the entire board would have to be replaced if a design change was needed. We join the discrete segment boards together by soldering a 0Ω resistor between the input/output signal traces, and PCB strips between the surrounding ground planes for structural integrity, with no resulting degradation to signal quality.

F. Scanning Synchronization System

As in previous iterations of the Holographic Monitor, horizontal scanning is achieved with a polygon mirror (such as those commonly used in laser printers), which reflects light onto a galvanometer mirror to be vertically scanned. In addition to scanning the output horizontally, the rotating mirror also descans (or "derotates") the output of the AOM as it traverses the LiNbO₃. Since we do not control the emission timing of the graphics card, the synchronization circuitry must precisely lock the scanning optical elements to the emitted GPU signals to produce a stationary output image. Otherwise, the output image will be incoherent.

The vertically-scanning galvanometer mirror is controlled by the graphics card's VSYNC signal and by a tachometer measuring the rotational rate of the polygon mirror. Every VSYNC pulse resets the galvanometer scan position to the top of the output image, and every tachometer pulse lowers the galvanometer scan position by a constant amount, such that the entire output image remains visible.

The horizontally-scanning polygon mirror is controlled by a hybrid hardware/software phase-locked loop; its reference signal being a division reduction of the graphics card HSYNC signal, and its process sense signal coming from a laser tachometer reflecting off of the rotating polygon mirror. The DC component of the polygon mirror motor control voltage is set by software (a Proportional-Integral Controller) and a digital-to-analog converter (DAC). The software replicates the normal operation of a PLL; adjusting the motor's control voltage until the rotational rate is approximately the same as the reference signal. A software PLL was chosen over a hardware PLL as it was considered to be more flexible. The AC component of the motor voltage is capacitor-coupled to the "PCP", or "Phase Comparator Pulse Output" pin of a 4046 chip (such as the MC74HC4046A). While this pin is usually used to indicate when a digital memory network ("type II") phase comparator is in lock (in a high-impedance state), it has been found that the PCP pin functionality, when used in this configuration, can lock the tachometer signal of the rotating polygon mirror to within ± 300 ns ($\pm 0.047\%$ of the period) of the divided HSYNC reference signal. When the tachometer signal is locked to the divided HSYNC signal, the image appears stationary.

The synchronization system is implemented on a single "shield" attachment circuit board connected to an Arduino MEGA 2560. The Arduino runs firmware that controls the scanning of the galvanometer mirror and the polygon mirror, based upon the VSYNC and HSYNC signals from the graphics card and from the polygon mirror tachometer. The Arduino is also used to re-flash the EDID data in an EEPROM chip on the DVI Breakout board, which is read by the host computer over the VGA / DVI interface to obtain precise display configuration parameters.

5. SOFTWARE IMPROVEMENTS

To produce images with the Holographic Monitor, we have developed a suite of software packages for testing and driving it. The code is developed in C++ with OpenFrameworks, a popular open-source, cross-platform multi-library wrapper [17]. Graphics card shader programming is done in GLUT (OpenGL Utility Toolkit) as it is natively supported in OpenFrameworks (although the Holographic Monitor does not restrict developers to this language alone). These programs are used for a variety of purposes and demonstrate algorithms that generate both stere-

ograms and holograms. To this point, we have only tested this software using a Microsoft Windows environment, but when compiled from source the software is likely portable to any operating system supported by OpenFrameworks. Graphical User Interfaces (GUIs) are used where possible to be user and developer friendly, intuitive, and to speed up experimentation cycles. All of our programs send output to the Monitor by having their output windows "full-screened" on the graphics card output connected to the Monitor's DVI Breakout Board.

A. Sweeper Testing Suite

The "Sweeper Suite" program is used for testing and verifying RF components and aligning the optical paths of the monitor. It generates single-tone frequencies on any or all of the separate color output channels of the graphics card in use. These frequencies can be adjusted manually or swept automatically across a defined frequency range. This is typically done to generate frequency response profiles of newly-built RF circuit boards and to show the optimal scanning range of the AOMs during alignment of post-modulator optics. Three frequencies can be generated concurrently and controlled separately, for use in interacting with red, green, and blue light.

The Sweeper Suite main GUI window includes options for setting frequency ranges and carrier frequencies independently for each output signal, taking into consideration the different frequency ranges within which red, green, and blue light is modulated by the modulators. Additionally, the sweep rate and current frequency can be manually adjusted using sliders, arrow keys, or direct numeric entry for easy and precise control. Each signal can also be enabled or disabled.

Distinct frequencies can be swept in unison to align the red, green, and blue modulator output angle ranges. The relative amplitude of each signal can be adjusted independently for color balance. These parameters are adjusted until the output of the red, green, and blue channels sweep in unison (converge) and produce a white-balanced output across an optimum range of angles. Once this criteria has been met, these frequency range and amplitude parameters are noted and used for other higher-order applications (such as those described below).

For an output with one signal per channel, the graphics card calculates pixel channel intensity values based upon the equation

$$I_c = A_c * \sin(O_{index} * \frac{f_c}{f_{GPU}} * 2\pi) * 0.5 + 0.5 \quad (5.1)$$

where c is the GPU color channel (red, green, or blue), I_c is the resulting pixel channel intensity (between 0-1), A_c is the chosen amplitude of a color channel (between 0-1), O_{index} is either x or $x + y * H_{Total}$, depending upon the GUI's "Time Coherent" setting, (x, y) are the output pixel coordinates, and f_c is the frequency of the tone to be generated.

For an output where three signals are combined into one channel (for FDCM modulators), averaging is used:

$$N = \sum_{c=\{r,g,b\}} A_c * \sin(O_{index} * \frac{f_c}{f_{GPU}} * 2\pi) \quad (5.2)$$

$$D = 3 \text{ or } \sum_{c=\{r,g,b\}} A_c \quad (5.3)$$

$$I_c = \frac{N}{D} * 0.5 + 0.5 \quad (5.4)$$

where A_r , A_g , and A_b are the amplitudes of the red, green, and blue tones, respectively. The method of calculating D can be set by the user in the GUI, depending upon whether absolute or relative amplitudes should be adjusted. The dynamic range of each signal is reduced to account for the GPU's finite range of pixel channel intensity values.

When testing radio frequency components, sections are connected to the DVI breakout board where Sweeper Suite signals are made available. These signals are swept to evaluate RF stage frequency responses, as measured by a spectrum analyzer. When aligning optical elements, a swept tone fed into an AOM yields a beam of light that moves across the deflection range of the modulator. This identifies the frequency and angular ranges of optimal brightness to be used and to align other optics against.

B. N-View Multimedia Stereogram Generator

Two-dimensional images and video streams can be displayed using our "Stereogram Generator" program. This program is used to project an arbitrary number of two-dimensional images (or video frames) at arbitrary horizontal output angles and positions from the Monitor. Video (either from a source file or a stream) is displayed by continuously updating the output images at the Holographic Monitor's frame rate, with little lag, permitting a video's original audio to accompany the Holographic Monitor output without modification.

This program renders two-dimensional images for the Holographic Monitor by amplitude-modulating a set of tones by a corresponding source image. For full-color images, three tones are chosen that, when passed through their respective modulators, project out of the Monitor at the same angle.

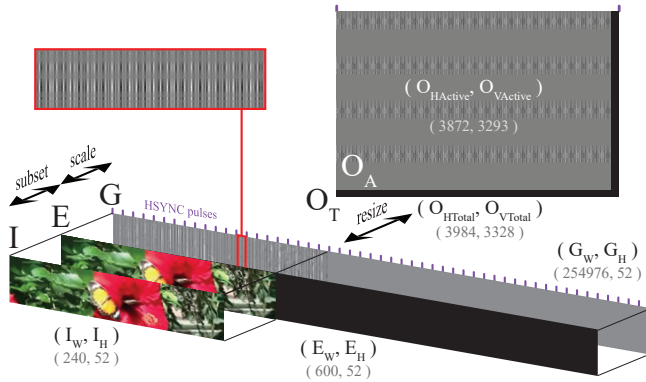


Fig. 8. Correlation of conceptual spaces in translating source images to Holographic Monitor output.

Figure 8 illustrates the relation between different sample spaces, and example dimensions in use at the time of this article's publication are included in subscripts. Space dimensions are described as (X_{Width}, X_{Height}) , where X is the space label. Space I , of size (I_W, I_H) , is the source image. Space E , of size (E_W, E_H) , is the effective output image space, representing what the output of the Monitor will look like. Note that because of various apertures within the Monitor, only approximately 40% of this space is displayed, mainly due to the wide 120° sweep of the 6-sided polygon mirror in use. Space G , of size (G_W, G_H) , is the grating space, containing each fringe pattern sample that will be sent to the AOM. (A 175×52 pixel sample of this is isolated in the upper left corner of Figure 8.) Space O is the output space, divided into a total output space, O_T , and a subset ac-

tive space, O_A . O_T is of size (H_{Total}, V_{Total}) , and O_A is of size (H_{Active}, V_{Active}) . The difference between O_T and O_A are minimal blanking regions demanded by the GPU's analog drivers. Samples of O_A are set by "full-screening" the program output window in the GPU output connected to the Holographic Monitor.

Spaces I , E , and G all have the same number of rows ($I_H = E_H = G_H = N_{HoloLines}$). The unit vector axes lengths of spaces I and E are equivalent, and I is a subset of E . E_W is experimentally determined to render an output image of equal aspect ratio to the source image. The maximum I_W permitted by the optical apertures is afterwards experimentally determined. A single row in both E and G correlate to the full sweep of a single polygon mirror facet, thus establishing a linearly-scaled relationship between their coordinate systems. From this, it can be calculated that $G_W = H_{Total} * N_{CRHL}$. Because graphics card hardware is produced to handle common aspect ratios (ie, 4:3, 16:9, etc...), and space G has an extremely wide aspect ratio (ie, 4903:1), space G is reshaped to space O_T (preserving the number of array elements while changing the width and height of the two-dimensional array). O_T is then cropped to O_A .

As graphics card cores can process individual pixels based upon pixel coordinates (O_i, O_j) and a set of global variables, a mapping from O_A to I is necessary. This mapping is described below:

$$O_x = O_j \text{ or } H_{Active} - 1 - O_j \quad (5.5)$$

$$y_{offset} = offset_x + offset_y * N_{CRHL} \quad (5.6)$$

$$O_y = O_i + y_{offset} \text{ or } V_{Active} - 1 - (O_i + y_{offset}) \quad (5.7)$$

$$O_{index} = O_x + O_y * H_{Total} \quad (5.8)$$

$$G_x = O_{index} \text{ mod } G_W \quad (5.9)$$

$$I_y = E_y = G_y = \text{floor}(O_{index} / G_W) \quad (5.10)$$

$$I_x = E_x = \text{floor}(G_x / G_W * E_W) \quad (5.11)$$

The variability in equations 5.5 and 5.7 are user configuration options if the image needs to be flipped. The variables $offset_x$ and $offset_y$ are used to adjust the position of the image on the output (with their respective space dimensions being $(N_{CRHL}, N_{HoloLines})$. All values are asserted to be within valid ranges, else, efforts to determine the corresponding sample in the source image are abandoned, and a default pixel intensity of 50% is used instead to maintain a constant signal average.

The intensity of output pixel $O_{A(O_i, O_j)}$ for separate red, green, and blue modulators is thus determined as:

$$sum_c = \sum_k^{N_{views}} I_{(k, I_x, I_y, c)} * W_{(k, c)} * \sin(O_{index} * \frac{f_{(k, c)}}{f_{GPU}} * 2\pi) \quad (5.12)$$

$$O_{A(O_i, O_j, c)} = \frac{sum_c}{N_{views}} * 0.5 + 0.5 \quad (5.13)$$

where N_{views} is the number of views (source images) composing the stereogram, $I_{(k, I_x, I_y, c)}$ is the intensity of color channel c of view k at coordinates (I_x, I_y) , $W_{(k, c)}$ is a white-balance weight for color channel c of view k , and $f_{(k, c)}$ is the frequency needed to project color channel c in the desired direction for view k .

Three-dimensional objects can be stereoscopically displayed using this program. A discrete set of translationally or rotationally-progressive renderings of the same 3D scene is loaded and set to display across a discrete continuum of output angles. The human subject in Figure 9 demonstrates this.

Viewers perceive parallax, and thus depth, as each eye receives a slightly different image. However, the discrete nature of stereogram views is noticeable, and no accommodation (focal) information is conveyed. Without appropriate focal distances, a stereographic image suffers from the Convergence-Accommodation Conflict [18], eventually leading to viewer discomfort.

A variant of this software has been developed to stream a desktop screen capture video feed. As one example, a popular four-player split-screen video game was run, and the stereogram-generating software was used to capture this stream, divide the four player view quadrants into separate streams, and to simultaneously project these streams from the same location on the Holovideo Monitor output in different directions, thus demonstrating viewer-specific specialized video feeds. Unfortunately we are unable to publicly show this demonstration due to the source material's copyright.

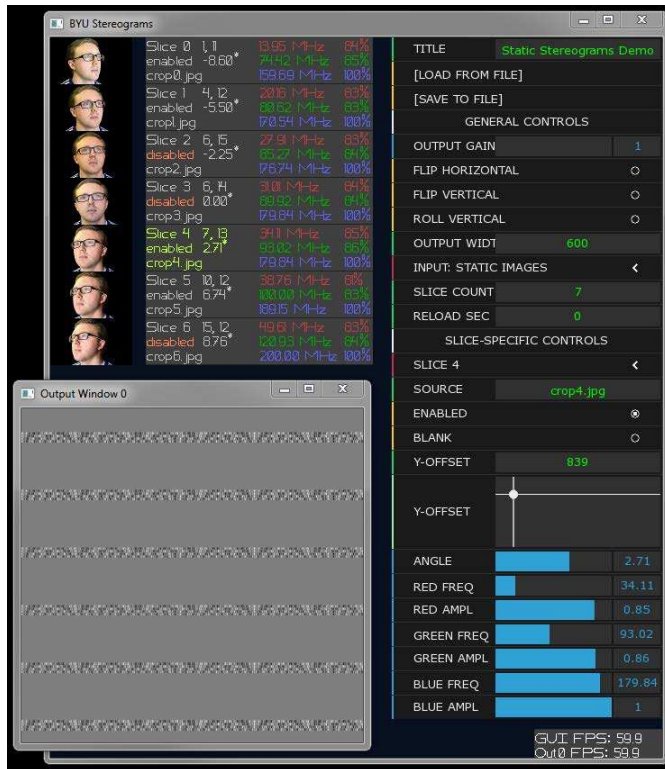


Fig. 9. The Stereogram generator GUI (background) and output window (foreground).

The GUI and output window of the Stereogram Generator, as shown in Figure 9, displays a list of stereogram views to be shown, and a number of widgets controlling global and view-specific variables. The frequency and white-balance weight for each color channel of each view can be adjusted here. Each view can be disabled, blanked, and translated as needed. Image and video filenames can be specified here, and JSON-format configuration files describing the entire program's state can be saved or loaded.

C. Hologram Generator

To test the holographic capabilities of the Holovideo Monitor, a simple raytracing algorithm was implemented to translate depth maps into the fringe patterns accepted by the Monitor. Although there is much optimization that could be applied to

this algorithm and better hologram-generation algorithms exist, it has successfully demonstrated parallax and accommodation.

Reusing the space notations established in the stereogram section and Figure 8, the effective image space E can be expanded into three-dimensional space by including a \hat{k} unit vector of equal length and units (pixels) with the \hat{i} and \hat{j} unit vectors of E . The algorithm creates a simple three-dimensional object in this expanded E space using a gray-scale depth map and intensity (color) map.

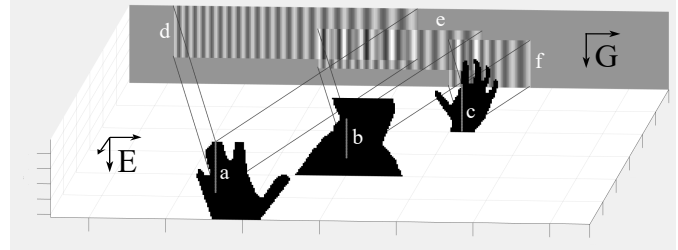


Fig. 10. An example of select points in extended E space projecting chirp patterns into G space.

For each depth map sample in space E , a corresponding sample range in the grating space G is calculated using the monitor's maximum angular deflection range. Between the limits of this sample range in G , a chirp is generated, with the instantaneous frequency along the chirp calculated to project light at an angle such that it intersects with the depth map sample being reconstructed in three-dimensional E space. The amplitude of this chirp is scaled by the intensity of the corresponding sample in the intensity map.

As an example, parts of a simple depth map are recreated in Figure 10. The depth map is of a person with two hands raised, the left-most hand brought towards the Monitor viewer and the right-most hand brought away, towards G . Samples along the gray columns next to markers a , b , and c in E each respectively project onto G to produce ranges d , e , and f . Each range progresses in frequency from those on the left that project light rightwards to those on the right that project light leftwards. In this example, frequencies that project light rightwards are high frequencies, and frequencies that project light leftwards are low frequencies.

This process is repeated for every sample in the depth map, with each chirp being added into G (as demonstrated by the overlapping regions of d , e , and f). The intensities of G are then clipped and scaled to the output range accepted by the graphics card, and reshaped into O_T and cropped to O_A . Rows in the depth/color map and E correspond directly to rows in G .

The pseudo-code of this algorithm for monochrome holograms in MATLAB[®] syntax is described in Listing 1:

Listing 1. Simple hologram-generating algorithm.

```
k_fr = freq_right / f_GPU * 2*pi;
k_fl = freq_left / f_GPU * 2*pi;
tan_half_angle = tan( angular_range / 2 );
G_W = H_Total * N_CRHL;
E_W = floor( N_HoloLines * 6.78 * 3 );
G = zeros( I_H, G_W );
```

```
for i = 1:I_H
    for j = 1:I_W
        if( cm(i, j) > 0 )
```

```

dm_j = dm(i, j);
half_chirp_width = tan_half_angle * dm_j;

e_l = j - I_W/2 - half_chirp_width;
e_r = j - I_W/2 + half_chirp_width;

g_l = floor( ( e_l/E_W + 1/2 ) * G_W );
g_r = floor( ( e_r/E_W + 1/2 ) * G_W );

for g_j = g_l:g_r
    r_j = g_j - g_l;
    f_alpha = r_j / ( g_r - g_l );
    f = f_alpha * ( k_fl - k_fr )/2 + k_fr;

    ci = cm(i, j)*sin( r_j*f );
    G(i, g_j+1) = ci + G(i, g_j+1);
end
end
end
end

```

*% clip and scale G values to output range of
% graphics card, then reshape G to O_T and
% crop to O_A, then display O_A in GPU output*

where *freq_right* and *freq_left* are the RF frequencies (in MHz) that cause the AOMs to project light at the right-most and left-most angles, respectively, and *angular_range* is the angular output range of the Monitor. I_W and I_H are the dimensions of the depth map source images.

6. RESULTS

At 52 HoloLines of vertical resolution, our current design still falls short of previously set goals. However, recent improvements have finally driven the bill of materials well below the goal of \$1000. The low cost of this design for the first time makes this architecture accessible to hobbyists. If provided with a functioning cartridge and software, only moderate assembly skill is needed to assemble the remainder of the system. By making our designs publicly available, we hope that our work can inspire continued development to make high-resolution, low-cost holographic video a reality.

To demonstrate accommodation and parallax, we displayed a sample grating generated by our holographic algorithm on the Monitor output. The monitor was placed on a freely-moving rotational stage, and a video camera recorded its output. The camera's focus was manually adjusted between subfigures *A* (closer focus) and *B* (farther focus) of Figure 11. Evidence of accommodation can be seen comparing all markers between *A* and *B*. When the camera is focused on the closer left hand in subfigure *A*, *c* exhibits detail, and *d* is blurred. When the camera is focused on the farther right hand in subfigure *B*, *c* is now blurred, and details such as the gaps between fingers can now be discerned in *d*. Between subfigures *B*-*D*, the monitor was rotated back and forth, simulating viewer head movement. Evidence of parallax can be seen by the varying widths of the gaps between objects of different depths (markers *a* and *b* in each subfigure), expanding and contracting as they would with a normal, three dimensional object.

While our design was created to accommodate three single color modulator cartridges, construction is still in progress on our first full-color Mark V monitor. As a proof of concept,

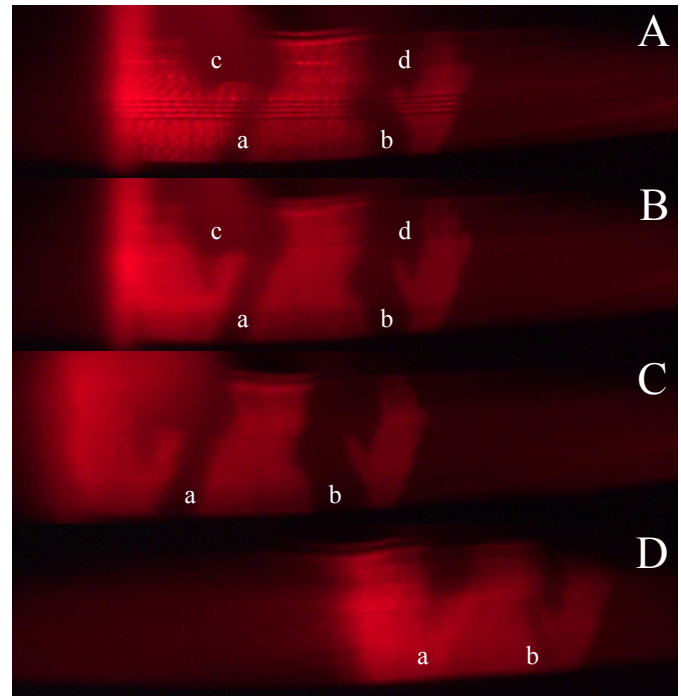


Fig. 11. Images demonstrating parallax and accommodation. For a more complete demonstration, see Visualization 1.



Fig. 12. A frame of a test color video (top) in reference to its equivalent 1-view stereogram Holographic Monitor output (bottom). See Visualization 2 for more detail.

we provide a demonstration of full color imagery via our stereogram software in Figure 12 using a previously-built and aligned FDCM Mark IV system.

A distinguishing feature of this architecture is the dramatically low cost relative to other holographic video platforms. Typically, designs relying on AOMs use off-the-shelf bulk wave modulators costing at least \$1000 on their own. Adding in the cost of driving electronics and optomechanical mounts, the materials cost alone restricted holographic displays to laboratories with significant research budgets. Now that the bill of materials is below \$1000 for the entire monitor (see Table 2), it can be budgeted for enthusiasts.

7. CONCLUSION

We present a full hardware and software system demonstrating low-cost, horizontal parallax-only holographic video. The system is based on scanned aperture holography first pioneered at MIT, with continued development at BYU. The original design for this architecture has existed for several years, but as yet has been prohibitively expensive, cumbersome, and mechanically unstable for consumer or hobbyist use, with a minimal amount

Table 2. Estimated Bill of Materials comparison of the BYU/MIT Mark IV Holographic Monitor and the new Mark V Holographic Monitor

Category	Mark IV	Mark V
Chassis	\$80	\$50
Optics	\$720	\$344
Modulator & Coupling	\$302	\$6
Electronics	\$420	\$420
Total	\$1522	\$820

of software developed to drive it. The most recent iteration addresses many of these drawbacks seeking to establish holographic video as a widely-accessible three-dimensional display.

Some significant changes were made to bring the bill of materials of this monitor down to the sub-\$1000 range. Most notable is the use of input coupling gratings to replace expensive rutile prism couplers. This also enabled the creation of a modular cartridge to enclose each modulator. Along with a size reduction, the cartridges and other 3D printed mounts stabilize the optical path, mitigating the vibration sensitivity in previous designs. With the optical path thus compacted, the chassis was likewise redesigned for ease of assembly and modularity, and to maximize the scanning aperture.

Beyond hardware enhancements, we present a suite of software packages designed to generate test signals and imagery for the Monitor using a conventional personal computer. Included are a sweep generator for testing and characterizing the electrical and optical elements, a multi-view stereogram generator capable of displaying images and video feeds, and an algorithm for computing display holograms based on depth map images.

In the future, many changes will be made to optimize our design further. We will continue to work on our modulators to improve efficiency and coupling. Target objectives include fabricating multi-channel modulators and revisiting single FDCM modulators that couple red, green, and blue light into the same channel. Multi-channel modulators would lead to increased resolution, and a single FDCM modulator could further decrease required space in the optical path and increase RF chain utilization. Optimizations to system bandwidth constraints could be made to reduce wasted bandwidth and increase visible resolution. Additionally, hardware changes may widen the available output bandwidth, thus increasing the resolution by other means. Further work on software will aim to achieve real-time rendering of holograms, a long-time ideal of computer-generated holography.

As understanding of the Holographic Monitor system is disseminated, techniques to incorporate new features, such as ultrasonic haptic interfaces and 3D cameras for augmented-reality interaction, will become apparent and made ripe for implementation. Other improvements to form factor and performance will help to make this system a viable 3D display solution, giving real, live, affordable holography to developers. Applications previously unimagined or confined to the realm of science fiction can now begin to flower from the untapped potential of tinkerers and hobbyists worldwide. With these publicly released designs, holographic video can now begin its exit from its laboratory-confined history and into mainstream adaptation.

The authors gratefully acknowledge development funding

generously provided by DAQRI LLC.

We also wish to acknowledge the contributions of alumni research group members who have previously contributed directly to the Holographic Monitor: Benjamin Haymore, Cameron Blocker, Zach Walker, Andy Dickinson, and Boyd Christiansen. We also wish to thank the assistance of our colleagues Jacob Kimball, Stephen McLaughlin, Kamran Qaderi, and Christopher Leach for their work on modulator design and general assistance.

REFERENCES

1. S. Gneiting, D. E. Smalley, K. Qaderi, A. Henrie, B. Haymore, S. McLaughlin, J. Kimball, C. Leach, and T. DeGraw, "Optimizations for robust, high-efficiency, waveguide-based holographic video," in *Industrial Informatics (INDIN), 2016 IEEE 14th International Conference on*, (IEEE, 2016), pp. 576–581.
2. K. Qaderi and D. E. Smalley, "Leaky-mode waveguide modulators with high deflection angle for use in holographic video displays," *Opt. Express* **24**, 20831–20841 (2016).
3. K. Qaderi, C. Leach, and D. E. Smalley, "Paired leaky mode spatial light modulators with a 28° total deflection angle," *Opt. Lett.* **42**, 1345–1348 (2017).
4. P. St-Hilaire, S. A. Benton, M. E. Lucente, and P. M. Hubel, "Color images with the mit holographic video display," (1992).
5. P. St-Hilaire, M. E. Lucente, J. D. Sutter, R. Pappu, C. J. Sparrell, and S. A. Benton, "Scaling up the mit holographic video system," (1995).
6. D. E. Smalley, Q. Y. J. Smithwick, and V. M. Bove, Jr., "Holographic video display based on guided-wave acousto-optic devices," (2007).
7. D. Smalley, Q. Smithwick, J. Barabas, V. M. B. Jr, S. Jolly, and C. DellaSilva, "Holographic for everyone: a low-cost holographic monitor," *Journal of Physics: Conference Series* **415**, 012055 (2013).
8. D. Henrie, B. Haymore, M. Zhang, D. Smalley, D. Alrabidi, S. Jolly, and V. M. Bove, "Progress on a low-cost holographic video monitor," in *Imaging and Applied Optics 2014*, (Optical Society of America, 2014), p. DW2B.3.
9. S. McLaughlin, C. Leach, S. Gneiting, V. M. Bove, S. Jolly, and D. E. Smalley, "Progress on waveguide-based holographic video (invited paper)," *Chin. Opt. Lett.* **14**, 010003 (2016).
10. VESA, "Enhanced extended display identification data standard," *Standard*, Video Electronics Standards Association (2000).
11. S. A. Gneiting, "Improved leaky-mode waveguide spatial light modulators for three dimensional displays," Master's thesis, Brigham Young University (2017).
12. D. E. Smalley, "Holographic on a stick: Integrated optics for holographic video displays," Ph.D. thesis, Massachusetts Institute of Technology (2013).
13. D. Smalley, Q. Smithwick, V. Bove Jr, J. Barabas, and S. Jolly, "Anisotropic leaky-mode modulator for holographic video displays," *Nature* **498**, 313 (2013).
14. S. McLaughlin, C. Leach, A. Henrie, and D. E. Smalley, "Optimized guided-to-leaky-mode device for graphics processing unit controlled frequency division of color," *Appl. Opt.* **54**, 3732–3736 (2015).
15. C. Leach, S. McLaughlin, A. Henrie, B. Haymore, and D. Smalley, "Design and fabrication of a color multiplexing linbo3 device," in *2015 IEEE 58th International Midwest Symposium on Circuits and Systems (MWSCAS)*, (2015), pp. 1–3.
16. S. McLaughlin, C. Leach, A. Henrie, D. Smalley, S. Jolly, and V. M. B. Jr., "Frequency division of color for holographic displays using anisotropic leaky mode couplers," in *Digital Holography & 3-D Imaging Meeting*, (Optical Society of America, 2015), p. DM2A.2.
17. "openframeworks," <http://openframeworks.cc/>. Accessed: 2017-07-07.
18. D. M. Hoffman, A. R. Girshick, K. Akeley, and M. S. Banks, "Vergence-accommodation conflicts hinder visual performance and cause visual fatigue," *Journal of Vision* **8**, 33 (2008).